2022 IEEE/RSJ International Conference on Intelligent Robots and Systems (IROS 2022)
October 23-27, 2022, Kyoto, Japan

Development of a Novel Low-profile Robotic Exoskeleton Glove for Patients with Brachial Plexus Injuries

Wenda Xu[1], Yujiong Liu[1] and Pinhas Ben-Tzvi[1*]

***Abstract*— This paper presents the design and development of a novel, low-profile, exoskeleton robotic glove aimed for people who suffer from brachial plexus injuries to restore their lost grasping functionality. The key idea of this new glove lies in its new finger mechanism that takes advantage of the rigid coupling hybrid mechanism (RCHM) concept. This mechanism concept couples the motions of the adjacent human finger links using rigid coupling mechanisms so that the overall mechanism motion (e.g., bending, extension, etc.) could be achieved using fewer actuators. The finger mechanism utilizes the single degree of freedom case of the RCHM that uses a rack-and-pinion mechanism as the rigid coupling mechanism. This special arrangement enables to design each finger mechanism of the glove as thin as possible while maintaining mechanical robustness simultaneously. Based on this novel finger mechanism, a two-finger low-profile robotic glove was developed. Remote center of motion mechanisms were used for the metacarpophalangeal (MCP) joints. Kinematic analysis and optimization-based kinematic synthesis were conducted to determine the design parameters of the new glove. Passive abduction/adduction joints were considered to improve the grasping flexibility. A proof-of-concept prototype was built and pinch grasping experiments of various objects were conducted. The results validated the mechanism and the mechanical design of the new robotic glove and demonstrated its functionalities and capabilities in grasping objects with various shapes and weights that are used in activities of daily living (ADLs).**

***Index Terms*— Rehabilitation Robotics, Exoskeleton Glove, Mechanism Design, Kinematics**

I. INTRODUCTION

Brachial plexus injury (BPI) is a severe peripheral nerve injury affecting upper extremities causing functional damage and physical disability [1]. Patients with such injuries suffer from a lack of muscle control and sensation in the arm, hand, and wrist. In addition, it has been proved that surgical options can restore the shoulder and arm functions, but much less so in returning sensation and mobility to the hand and wrist [2].

Recent studies have found that using exoskeleton devices is a promising way to help patients to restore their functional abilities for activities of daily living (ADLs). As discussed in [3], the exoskeleton robotic hand should contain a compact design, a simple mechanism, and good ergonomics (e.g., remote center of motion, self-aligning joints, etc.). However, previous designs of soft robotic gloves [4]–[6], cable-driven gloves [7], [8], and linkage-driven gloves [9], [10], did not fully meet such requirements. The bulky design of the robotic hand shapes, the large weight of the system, and the need for multiple actuators, are the most common shortcomings of these designs. The three main criteria (wearability, comfortability, and portability) to evaluate a robotic glove are still not satisfied by existing designs.

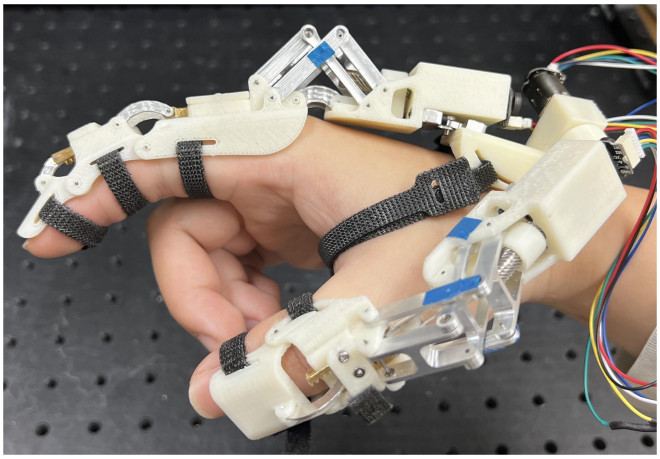

Fig. 1. A proof-of-concept prototype of the new exoskeleton glove.

To improve the performance of the robotic gloves in terms of wearability, comfortability, and portability, we propose a new two-digit exoskeleton glove design that is compact, low-profile, portable, and functional for ADLs for patients by considering both the general requirements of hand exoskeleton devices and the shortcomings of existing wearable devices. Fig. 1 shows a proof-of-concept prototype of this new exoskeleton glove. Each finger linkage is driven by a customized linear actuator. Different links of each exoskeleton finger are connected by using the rigid coupling hybrid mechanism (RCHM), which couples their motions to reduce the number of degrees of freedom (DOF). The proposed exoskeleton glove also takes the thumb motion into account. The synthesized mechanism imitates the human hand motion and increases the device's wearability and comfortability.

The main contributions of this work are summarized as follows. Firstly, a novel low-profile, two-digit exoskeleton glove mechanism is proposed. Secondly, kinematic analysis and optimization-based kinematic synthesis for this new mechanism are presented to determine the critical design parameters. Thirdly, a proof-of-concept prototype was built and grasping experiments with various objects were conducted to evaluate the proposed robotic glove. Compared with other

Research reported in this publication was supported by the Eunice Kennedy Shriver National Institute of Child Health & Human Development of the National Institutes of Health under Award Number R21HD095027. The content is solely the responsibility of the authors and does not necessarily represent the official views of the National Institutes of Health.

[1]Wenda Xu, Yujiong Liu, and Pinhas Ben-Tzvi are with the Robotics and Mechatronics Lab in the Mechanical Engineering Department, Virginia Tech, Blacksburg, VA 24060, USA {wenda, yjliu, bentzvi}@vt.edu

*Corresponding author

hand exoskeletons, the unique characteristics of the new glove include: (1) the glove mechanism is based on linkage transmission (including rack-and-pinion mechanism), which is mechanically stable and robust; (2) the finger mechanism is based on the RCHM concept which results in a low-profile and compact design, (3) the glove is synthesized based on imitating the actual human hand motion, which provides better grasping performance for ADLs for patients. The integrated actuators also improve the portability of the entire exoskeleton glove.

The rest of this paper is organized as follows. In section II, the mechanism and mechanical design of the exoskeleton glove are presented. In section III, the kinematic model of the exoskeleton glove is derived. Section IV introduces the optimization-based kinematic synthesis method that imitates the human hand grasping motion. In Section V, the prototyping and grasping experiments of the proposed exoskeleton glove are presented to evaluate its performance. Potential problems and future work are also discussed in this section. Lastly, section VI concludes the paper.

II. Mechanism and Mechanical Design

The proposed exoskeleton glove takes advantage of the coupling motion between different phalanges on each finger while grasping. Considering the results from previous research [11]–[13] that the hand with reduced DOFs is sufficient to perform most of the grasping motions for ADLs, the three DOFs of each finger (excluding the abduction-adduction) can be simplified to one. The simplified exoskeleton finger requires fewer actuators and thus it is lighter. The proposed exoskeleton glove adopts this idea and the single DOF finger mechanism is designed based on the one DOF case of the rigid coupling hybrid mechanism (RCHM) concept [14] with a rack-and-pinion mechanism as the rigid coupling mechanism (RCM). This special design is able to make the finger mechanism as thin as possible which improves the wearability, comfortability, and the portability of the new glove.

The RCHM is used to address the difficulties in transmitting motion for serially connected spatial mechanisms. The core idea is to couple the motion of the i-th link with $i+1$-th link. The motion of the current link is driven by its adjacent links instead of the actuator. This special driving mechanism causes the motion of the actuator to be propagated to the end link by pushing its next link sequentially. To achieve this effect, the RCHM requires two basic components: one parallel mechanism (PM) determining the basic mobility of the mechanism and one RCM that couples the motions of the adjacent PMs. The RCM could be implemented in various forms (e.g., rack-and-pinion, four-bar mechanism, etc.) depending on the actual design requirements. The proposed novel finger mechanism utilized two pairs of the offset slider-crank mechanism as the PM and one rack-and-pinion mechanism as the RCM. Fig. 2 shows these two building block mechanisms of the novel single DOF finger mechanism.

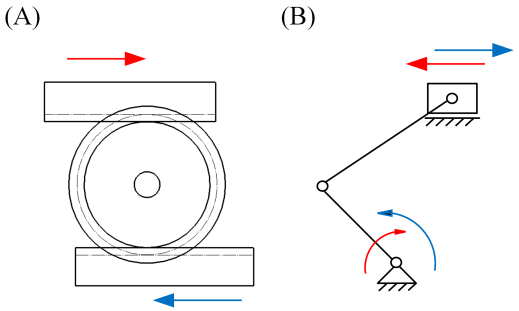

Fig. 2. The two mechanism elements and the motions of the new finger mechanism: (A) a rack-and-pinion mechanism for motion reversing; (B) an offset slider-crank mechanism for motion conversion. The red arrow represents the input and the blue arrow represents the output.

The design overview of the proposed novel exoskeleton glove is shown in Fig. 3. The index finger exoskeleton consists of three links: a distal phalanx, a middle phalanx, and a proximal phalanx, as well as three relative joints, including a distal interphalangeal (DIP), a Proximal interphalangeal (PIP), and a metacarpophalangeal (MCP) joint. The thumb exoskeleton is similar except for the middle phalanx and DIP joint. To make the exoskeleton glove fit the hand properly, each link of the exoskeleton finger covers the corresponding phalanx on the human hand and each joint coincides with the corresponding joint on the human hand. The passive abduction and adduction mechanism (indicated by green arrows) is also added for each finger to provide a comfortable experience for the wearers.

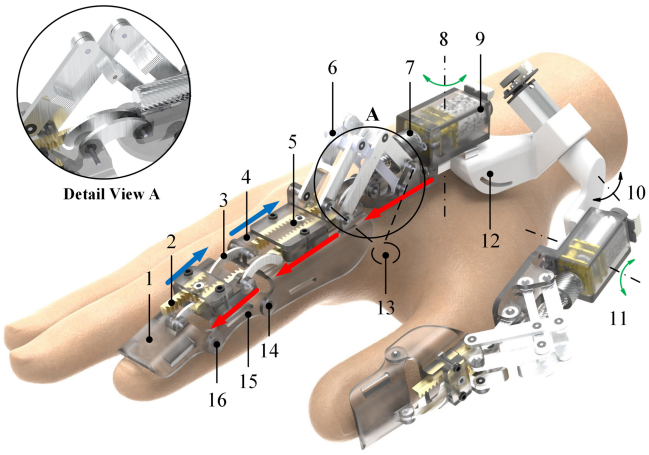

1. Distal Link
2. Rack
3. Connector
4. Proximal Link
5. Gear
6. Remote Center of Motion
7. Leadscrew Nut
8. Passive Abd-adduction Axis
9. Linear Actuator
10. Thumb Rotation Axis
11. Passive Abd-adduction Axis
12. Base
13. MCP Joint (Virtual)
14. PIP Joint
15. Middle Link
16. DIP Joint

Fig. 3. Overview of the exoskeleton glove assembly. The detailed view A shows how the linear actuator is connected to the Proximal link. The red arrow shows the "Driving" mechanism and the blue arrow shows the "Measuring" mechanism.

Different links are connected by a series of offset slider-crank mechanisms and rack-and-pinion mechanisms. The principles of the finger mechanism are explained as follows. From the motor side, the leadscrew nut of the linear actuator

is connected with the Proximal link through a connector. The linear actuator, the connector, the Proximal link, and the MCP joint form the first offset slider-crank mechanism, which converts the linear motion generated by the linear actuator to a rotary motion of the MCP joint and drives the Proximal link accordingly. In addition, the housing of the linear actuator is connected to the sliding rack by another connector. The housing of the linear actuator, the connector, the rack, and the MCP joint forms the second offset slider-crank mechanism, which converts the rotary motion of the MCP joint to the linear motion of the rack. Therefore, the motion which starts from the linear actuator, is transmitted to the linear motion of the rack on the Proximal link, with a different direction, by the rotation of the MCP joint. It is worth mentioning that the MCP joint on the exoskeleton finger is virtual and replaced by the Remote Center of Motion mechanism to avoid interference with the hand.

The first offset slider-crank mechanism with forward motion is defined as the "Driving" mechanism (red arrow in Fig. 3) since it drives the next link's motion. The second offset slider-crank mechanism with backward motion is defined as the "Measuring" mechanism (blue arrow in Fig. 3) since its motion depends on the "Driving" mechanism and it "measures" the output motion of the first link. Here, the rotation angle of the MCP joint generated by the "Driving" mechanism is measured by the "Measuring" mechanism and presented as the displacement of the rack. Similarly, there is another pair of "Driving" and "Measuring" mechanisms around the PIP joint. The rack-and-pinion mechanism connects the first "Measuring" mechanism to the second "Driving" mechanism, which results in the coupling motion between the MCP joint and the PIP joint. Thereby, the motion of the linear actuator is sequentially transmitted to the end effector (distal link). It is worth noting that there is no "Measuring" mechanism around the DIP joint since it is already connected to the last link.

III. Kinematic Analysis

As shown in Fig. 4, the hand kinematics includes the index finger kinematic chain and the thumb kinematic chain. Since different finger joints (planar motion) have a similar coupling motion, their kinematics are summarized into one formulation (Section III-A). The spatial kinematic chain from the base to the thumb Metacarpal link is treated separately (Section III-B).

A. Finger Linkage Kinematic Analysis

Since different fingers utilize the same mechanism, for the finger linkage kinematic analysis, we have chosen the index finger as an example. The forward kinematic chain of the index finger is given by:

$$\begin{aligned} p_x + ip_y =& l_p e^{i\theta_{mcp}} + l_m e^{i(\theta_{mcp}+\theta_{pip})} \\ &+ l_d e^{i(\theta_{mcp}+\theta_{pip}+\theta_{dip})} \end{aligned} \tag{1}$$

where p_x, p_y are the x and y coordinates of the finger end point position in the finger bending plane. θ_{MCP}, θ_{DIP}, and θ_{PIP} are the rotating angles of the MCP joint, the PIP joint, and the DIP joint, respectively. l_p, l_m and l_d are the lengths of the Proximal link, the Middle link, and the Distal link, respectively.

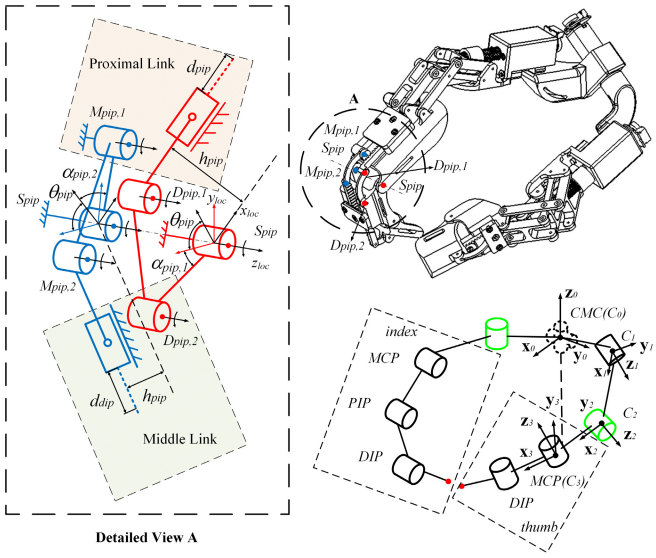

Fig. 4. Kinematic model of the exoskeleton glove mechanism. Detailed view A shows the kinematic model around the PIP joint on the index finger.

The kinematic model of the proposed finger exoskeleton mechanism consists of two and a half pairs of serially connected "Driving" and "Measuring" chains as discussed in Section II. Since both the "Driving" and the "Measuring" chains of each pair perform the same rotation around the corresponding finger joint, the following relationship can be obtained:

$$A_{jnt,i} = \sqrt{B_{jnt,i}^2 - C_{jnt,i}^2} + D_{jnt,i} - E_{jnt,i} \tag{2}$$

where

$$A_{jnt,i} = (l_{jnt,i} - d_{jnt}) \cos \alpha_{jnt,i} \tag{3}$$
$$B_{jnt,i} = l_{jnt,i}^2 \cos \alpha_{jnt,i} \tag{4}$$
$$C_{jnt,i} = h_{jnt}^2 (\cos \alpha_{jnt,1} - cos(\alpha_{jnt,i} + \theta_{jnt})) \tag{5}$$
$$D_{jnt,i} = h_{jnt} \sin \alpha_{jnt,i} \tag{6}$$
$$E_{jnt,i} = h_{jnt} \cos(\alpha_{jnt,i} + \theta_{jnt}) \tag{7}$$

and $jnt \in \{mcp, pip, dip\}$, $i \in \{1, 2\}$. Subscript $i = 1$ refers to the "Driving" chain and subscript $i = 2$ refers to the "Measuring" chain. More specifically, a pair of the "Driving" chain and the "Measuring" chain around the PIP joint (Detailed view A in Fig. 4) is selected to illustrate the kinematic parameters. $l_{pip,1}$ is the link length from $D_{pip,1}$ to $D_{pip,2}$. $l_{pip,2}$ is the link length from $M_{pip,1}$ to $M_{pip,2}$. d_{dip} is the displacement of the rack in the "Driving" chain. h_{pip} is the distance between the PIP joint and the middle plane of the rack. $\alpha_{pip,2}$ is the pre-rotation angle of the link starting from $M_{pip,1}$ to S_{pip} with respect to the z_{loc} axis.

Different pairs of the "Driving" and "Measuring" chains are connected by the rack-and-pinion mechanism. All pinions (0.5 Modulus) and racks (0.5 Modulus, 10 Teeth) are chosen to be the same to simplify the design, which results in the rack of the current "Driving" chain sharing the same

displacement with the rack of the previous "Measuring" chain. This way, the motion of different pairs of chains are coupled. With the input position of the linear actuator, the final position of the Distal link can be calculated correspondingly.

B. Thumb Kinematic Analysis

The human thumb consists of three links, which are the Proximal link, the Distal Link, and the Metacarpal link. The kinematics of the first two links (dashed block in Fig. 4) are covered by the aforementioned finger linkage kinematics since they are connected with the interphalangeal (IP) and the MCP joint, which only has one DOF. In this section, we only discuss the kinematics from the Carpus (the base link) to the Metacarpal link.

Because the Metacarpal link is connected to the Carpus with the Carpo-Metacarpal (CMC) joint which provides 2 DOFs, the CMC joint is divided into two independent revolute joints ($C1$ and $C2$) on the exoskeleton to mimic its functionalities as shown in Fig. 4. It should be noted that the second revolute joint ($C2$) is designed to be passive so that it is consistent with other finger exoskeletons.

Since the CMC joint on the thumb and the CMC joint on the index finger are closely attached, the CMC (C_0) joint on the thumb is selected as the origin of the global coordinates. The j-th link frame $\sum C_j := (C_j, \mathbf{x}_j, \mathbf{y}_j, \mathbf{z}_j)$, $(0 \leq j \leq 3)$ is defined at the joint j axis, with $\mathbf{z}_j$ coinciding joint j axis and $\mathbf{x}_j$ pointing to the next joint. The forward kinematics from the CMC joint on the hand to the MCP joint on the thumb can be then expressed as

$$\mathbf{R}_{C_j} = \mathbf{R}_{C_{j-1}} \mathbf{R}_z(\beta_{C_j,z}) \mathbf{R}_y(\beta_{C_j,y}) \mathbf{R}_x(\beta_{C_j,x}) \mathbf{R}_z(\theta_{C_j}) \tag{8}$$

$$\mathbf{p}_{C_j} = \mathbf{R}_{C_{j-1}} \mathbf{p}_{C_{j-1},C_j} + \mathbf{p}_{C_{j-1}} \tag{9}$$

where $\mathbf{R}_{C_j}$ denotes the orientation of the frame $\sum C_j$, $\mathbf{R}_x(\cdot)$, $\mathbf{R}_y(\cdot)$, and $\mathbf{R}_z(\cdot)$ denote the principle rotation matrix functions with respect to the corresponding axis, $\boldsymbol{\beta}_{C_j} = [\beta_{C_j,x}\ \beta_{C_j,y}\ \beta_{C_j,z}]^T$ denotes the vector of rotation angles with respect to the corresponding axis, θ_{C_j} denotes the rotation angle of the joint C_j, $\mathbf{p}_{C_j}$ denotes the C_j position, $\mathbf{p}_{C_{j-1},C_j}$ denotes the vector from C_{j-1} to C_j. For the initial conditions, $\mathbf{R}_{C_0}$ is the identity matrix, θ_{C_0} is zero, $\mathbf{p}_{C_0}$ and $\boldsymbol{\beta}_{C_0}$ are zero vectors.

IV. Kinematic Synthesis

The finger mechanism requires each joint axis on the exoskeleton to coincide with the joint axis on the human finger. Because of the large size and shape variations for individual human fingers, the optimization is performed based on the first author's finger dimensions as shown in Table I. It should be noted that the thumb does not have the middle link and the l_c for the index finger is ignored since it has little impact on the finger motion. The feasibility of designing for different finger sizes will be discussed in Section VI.

TABLE I
Finger Dimensions

Name	l_c (mm)	l_p (mm)	l_m (mm)	l_d (mm)
index	-	50.0	27.2	26.4
thumb	52.0	36.0	-	34

The proposed exoskeleton glove is designed to realize the natural grasping motion of the human hand. Therefore, design variables of the exoskeleton glove should be optimized to imitate natural grasping motion. The UNIPI dataset [15] was used as the human motion reference because it is more accurate and elaborate. It contains the trajectories of each finger joint while grasping. The finger joint data of grasping the No. 8 object with respect to the No. 1 subject is selected due to its long trajectories of the joints motion, which helps to enlarge the workspace of the exoskeleton glove. Since each trajectory contains thousands of points that cover both the grasping and the releasing motion, the data is pre-processed to include only the grasping motion. From the grasping data, four positions that are equally distributed on the path are selected as the landmarks. Each landmark contains six joint angles (index: MCP, PIP, DIP; thumb: CMC, MCP, DIP) to define the posture of the hand.

The goal of the optimization is to minimize the difference between the exoskeleton glove trajectory and the human motion trajectory. Therefore, the objective function is designed as the root mean squared error $\mathbf{e} \in \mathbb{R}^{24\times 1}$ between the joint angles of the landmarks and the joint angles of the exoskeleton fingers with different weights $\mathbf{w}_k \in \mathbb{R}^{1\times 6}$ for the k-th $(1 \leq k \leq 4)$ landmark. The objective function is defined as

$$obj := [\mathbf{w}_1 \quad \mathbf{w}_2 \quad \mathbf{w}_3 \quad \mathbf{w}_4]\mathbf{e} \tag{10}$$

The weights selection for the MCP, PIP, and DIP joints considers the different range of motion of each joint and its relationship with the adjacent joints [16],

$$0^\circ \leq \theta_{mcp} \leq 90^\circ \tag{11}$$

$$0^\circ \leq \theta_{pip} \leq 110^\circ \tag{12}$$

$$0^\circ \leq \theta_{dip} \leq 90^\circ \tag{13}$$

$$\theta_{dip} = \frac{2}{3}\theta_{pip} \tag{14}$$

After several experiments, we chose the equally weights for different positions and different weights for each joint $(\mathbf{w}_1 = \mathbf{w}_2 = \mathbf{w}_3 = \mathbf{w}_4 = [1, 2, 1, 2, 1, 1])$.

The thumb and index finger are optimized together to achieve a better performance. Equations (2)-(9) are employed as the equality constraints. It is worth mentioning that the rotation angle of the passive joint (C_2) on the thumb is set to zero during the optimization. This constraint is set as the soft constraint to minimize the motion of the uncontrollable parts while grasping. For the finger linkage mechanism, the following nonlinear inequality constraints are added to

accommodate the rack-and-pinion mechanisms,

$$2d_{pip} \leq l_p - h_{mcp}cos(\alpha_{mcp,1}) - h_{pip}\cos(\alpha_{pip,2}) \quad (15)$$

$$2d_{dip} \leq l_m - h_{pip}\cos(\alpha_{pip,1}) - h_{dip}\cos(\alpha_{dip,2}) \quad (16)$$

$$h_{pip} \leq h_{mcp} \quad (17)$$

$$h_{dip} \leq h_{pip} \quad (18)$$

The optimization problem is solved by the MATLAB function `fmincon` with the "interior-point" algorithm. The optimized design variables are collected in Table II.

TABLE II
OPTIMIZED DESIGN VARIABLES

Index Finger			
Variable	Value	Variable	Value
$l_{mcp,1}$	13.0 mm	$l_{mcp,2}$	13.9 mm
$l_{pip,1}$	15.0 mm	$l_{pip,2}$	15.6 mm
$l_{dip,1}$	8.2 mm	h_{mcp}	16.7 mm
h_{pip}	10.0 mm	h_{dip}	10.0 mm
$\alpha_{mcp,1}$	17.1 deg	$\alpha_{mcp,2}$	22.3 deg
$\alpha_{pip,1}$	24.6 deg	$\alpha_{pip,2}$	30.0 deg
$\alpha_{dip,1}$	30.0 deg		
Thumb			
$l_{mcp,1}$	14.9 mm	$l_{mcp,2}$	20 mm
$l_{dip,1}$	15.9 mm	h_{mcp}	16.1 mm
h_{dip}	10.0 mm	$\alpha_{mcp,1}$	17.2 deg
$\alpha_{mcp,2}$	10.0 deg	$\alpha_{dip,1}$	30.0 deg
$p_{C_0,C_1,x}$	-14.8 mm	$\beta_{C_1,x}$	-154.5 deg
$p_{C_0,C_1,y}$	10.1 mm	$\beta_{C_1,y}$	-170.2 deg
$p_{C_0,C_1,z}$	16.3 mm	$\beta_{C_1,z}$	-128.8 deg
$p_{C_1,C_2,x}$	2.9 mm	$\beta_{C_1,x}$	115.7 deg
$p_{C_1,C_2,y}$	-24.0 mm	$\beta_{C_1,y}$	170.4 deg
$p_{C_1,C_2,z}$	-18.6 mm	$\beta_{C_1,z}$	38.6 deg
l_{C_2,C_3}	40.0 mm		

For a better illustration of the optimization results, Fig. 5 shows the trajectory comparisons between the optimized exoskeleton glove and the human hand. The reference hand trajectories are generated by taking the joints' angles from a data set, and reconstructing with the same kinematics against the phalanx lengths. The results show that the optimized trajectories properly follow the actual human hand trajectories from the start of the motion to the end of the motion. For the thumb that uses two separate joints to mimic the CMC joint, the exoskeleton glove is still able to follow the desired human hand motion.

V. PROTOTYPING AND EXPERIMENTS

Based on the synthesized results, a proof-of-concept prototype exoskeleton glove was designed and manufactured. Each link of the exoskeleton finger is 3D printed using acrylonitrile butadiene styrene (ABS). The connectors are made out of 6061T6 aluminum alloy. The racks and pinions are

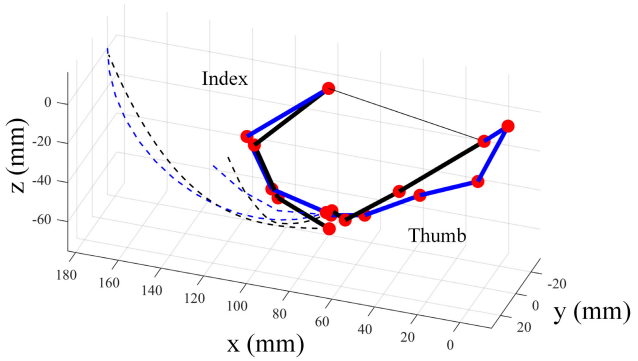

Fig. 5. Optimization results of the exoskeleton glove. The black bars denote the phalanges of the human finger of and the blue bars denotes the exoskeleton link. The red dots denote the joints. The blue dashed lines and black dashed lines are the end point trajectories of the reference hand motion and the end point trajectories of the exoskeleton glove, respectively. It can be found that the difference between the optimized trajectories and actual human hand trajectories is fairly small.

manufactured by customizing off-the-shelf 0.5 modulus brass gears and racks. The linear actuators are customized using a leadscrew (lead=20mm, starts=16, pitch diameter=5.5mm, thread angle=30°, lead angle=49.27°) and a direct current (DC) motor with gearbox that provides a torque constant of 980 N·mm, a normal speed of 35 RPM, and a 1000 : 1 reduction ratio. 681 miniature bearings are used for all the rotating joints. Each link is attached with Velcro to bind it securly on the patient's finger. The total mass of the prototype is 110 grams.

The motor controller uses the same hardware and software as in the previous project [17], which consists of a Teensy 4.1 Microcontroller Unit (MCU) and three TB6612FNG motor drivers. The motor controllers of all three motors run in parallel at 10Hz on the MCU with a FreeRTOS embedded operating system to ensure minimal control latency. The overall position control is realized by the common proportional–integral–derivative (PID) controller. The motor controller is connected to the power supply directly.

Four different kinds of daily used objects with different shapes (cylinder, sphere, cube) were selected to test the performance of the proposed exoskeleton glove. A healthy subject was involved in the experiments to wear the exoskeleton glove and perform the pinch grasp three times on the goal object without any intentional movement. Each grasp trial includes 3 steps: grasping the goal object from the table, holding the object for a few seconds, and releasing the object.

Fig. 6 shows the grasp performance while wearing the proposed exoskeleton glove. The result shows that the glove has the ability to help the subject grasp and hold the goal objects. The motion of each finger follows the optimized trajectories. The large workspace provides the ability to grasp different types of objects. Objects with flat surfaces could be easily grasped by the skeleton glove. However, for objects with round and smooth surfaces, such as a small ball and pen, the object easily slipped away while the exoskeleton was applying the grasping force on the object. This issue

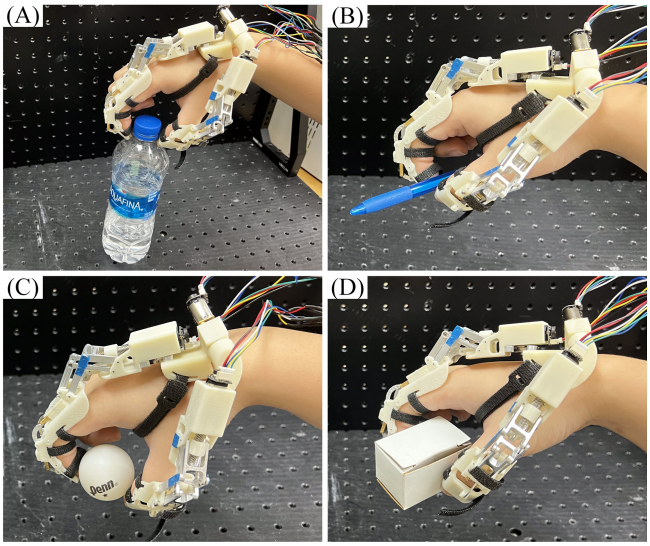

Fig. 6. Four successful grasping on various objects: (A) bottle, (B) pen, (C) ball, (D) box.

could be solved in future work by increasing the contact friction on the fingertips.

Another two subjects who have similar hand size could also wear the proposed exoskeleton glove and perform the same tasks. This proves that our customized exoskeleton glove is able to accommodate a range of people with similar hand size.

Potential problems associated with the proposed exoskeleton glove were also identified. Due to the long kinematic chain on each finger, the errors on the design variables were accumulated on the fingertips, which reduced the motion accuracy. Moreover, the backlash between the rack and the pinion as well as the friction force between the rack and its housing reduce the performance of the glove. In addition, due to the large motion range of the PIP joint, the offset slider-crank mechanism should be designed carefully to avoid its singular positions.

VI. Conclusion And Future Work

In this paper, we presented a novel exoskeleton glove mechanism that has a low-profile, compact, and portable design feature for individuals with hand disabilities, to assist their activities of daily living and for rehabilitation. Mechanism and mechanical design were presented first. Kinematic analysis and kinematic synthesis of the novel mechanism for a better alignment with the actual human hand motion were then conducted. The optimized exoskeleton achieved a similar motion as a human finger for grasping objects. The glove and the actuators were integrated and mounted on the back of the hand to avoid external actuation. A proof-of-concept prototype was then built and grasping experiments were performed. The experiments demonstrated the new mechanism's ability to grasp daily used objects with dexterity. However, it also revealed some design issues with the existing prototype. Overcoming these drawbacks will be a major focus of the future work. The integration of force sensors to provide force control instead of using the position control will also be investigated. Further research on the force control and the development of a five-digit exoskeleton glove is also an aspect of our future work.

References

[1] H. R. Park, G. S. Lee, I. S. Kim, and J.-C. Chang, "Brachial Plexus Injury in Adults," *The Nerve*, vol. 3, no. 1, pp. 1–11, 2017.

[2] J. L. Giuffre, S. Kakar, A. T. Bishop, R. J. Spinner, and A. Y. Shin, "Current Concepts of the Treatment of Adult Brachial Plexus Injuries," *Journal of Hand Surgery*, vol. 35, no. 4, pp. 678–688, 4 2010.

[3] J. Iqbal, N. Tsagarakis, A. E. Fiorilla, and D. Caldwell, "Design requirements of a hand exoskeleton robotic device," in *14th IASTED International Conference on Robotics and Applications (RA), Massachusetts US*, vol. 664, no. 81, 2009, pp. 44–51.

[4] P. Polygerinos, Z. Wang, K. C. Galloway, R. J. Wood, and C. J. Walsh, "Soft robotic glove for combined assistance and at-home rehabilitation," *Robotics and Autonomous Systems*, vol. 73, pp. 135–143, 2015.

[5] H. K. Yap, B. W. Ang, J. H. Lim, J. C. Goh, and C. H. Yeow, "A fabric-regulated soft robotic glove with user intent detection using EMG and RFID for hand assistive application," in *Proceedings - IEEE International Conference on Robotics and Automation*, vol. 2016-June. Institute of Electrical and Electronics Engineers Inc., 6 2016, pp. 3537–3542.

[6] A. Borboni, M. Mor, and R. Faglia, "Gloreha-Hand Robotic Rehabilitation: Design, Mechanical Model, and Experiments," *Journal of Dynamic Systems, Measurement and Control, Transactions of the ASME*, vol. 138, no. 11, 11 2016.

[7] Z. Ma, P. Ben-Tzvi, and J. Danoff, "Sensing and Force-Feedback Exoskeleton Robotic (SAFER) Glove Mechanism for Hand Rehabilitation," *Proceedings of the ASME Design Engineering Technical Conference*, vol. 5A-2015, pp. 1–8, 2015.

[8] U. A. Hofmann, T. Bützer, O. Lambercy, and R. Gassert, "Design and Evaluation of a Bowden-Cable-Based Remote Actuation System for Wearable Robotics," *IEEE Robotics and Automation Letters*, vol. 3, no. 3, pp. 2101–2108, 2018.

[9] D. Leonardis, M. Barsotti, C. Loconsole, M. Solazzi, M. Troncossi, C. Mazzotti, V. P. Castelli, C. Procopio, G. Lamola, C. Chisari, M. Bergamasco, and A. Frisoli, "An EMG-controlled robotic hand exoskeleton for bilateral rehabilitation," *IEEE Transactions on Haptics*, vol. 8, no. 2, pp. 140–151, 2015.

[10] N. S. Ho, K. Y. Tong, X. L. Hu, K. L. Fung, X. J. Wei, W. Rong, and E. A. Susanto, "An EMG-driven exoskeleton hand robotic training device on chronic stroke subjects: Task training system for stroke rehabilitation," in *IEEE International Conference on Rehabilitation Robotics*, 2011.

[11] G. A. Bekey, R. Tomovic, and I. Zeljkovic, "Control architecture for the belgrade/usc hand," in *Dextrous robot hands*. Springer, 1990, pp. 136–149.

[12] Z. Ma, P. Ben-Tzvi, and J. Danoff, "Hand Rehabilitation Learning System with an Exoskeleton Robotic Glove," *IEEE Transactions on Neural Systems and Rehabilitation Engineering*, vol. 24, no. 12, pp. 1323–1332, 2016.

[13] E. Refour, B. Sebastian, and P. Ben-Tzvi, "Two-digit robotic exoskeleton glove mechanism: Design and integration," *Journal of Mechanisms and Robotics*, vol. 10, no. 2, 4 2018.

[14] Y. Liu and P. Ben-Tzvi, "Design, analysis, and integration of a new two-degree-of-freedom articulated multi-link robotic tail mechanism," *Journal of Mechanisms and Robotics*, vol. 12, no. 2, p. 021101, 2020.

[15] C. Della Santina, M. Bianchi, G. Averta, S. Ciotti, V. Arapi, S. Fani, E. Battaglia, M. G. Catalano, M. Santello, and A. Bicchi, "Postural hand synergies during environmental constraint exploitation," *Frontiers in Neurorobotics*, vol. 11, no. August, pp. 1–14, 2017.

[16] J. Lin, Y. Wu, and T. S. Huang, "Modeling the constraints of human hand motion," *Proceedings - Workshop on Human Motion, HUMO 2000*, pp. 121–126, 2000.

[17] Y. Guo, W. Xu, S. Pradhan, C. Bravo, and P. Ben-Tzvi, "Personalized voice activated grasping system for a robotic exoskeleton glove," *Mechatronics*, vol. 83, p. 102745, 2022.